Atomistic Simulation of the α_c-Relaxation in Crystalline Polyethylene

Shawn W. Mowry and Gregory C. Rutledge*

Department of Chemical Engineering, Massachusetts Institute of Technology, Cambridge, Massachusetts 02139

Received October 26, 2001; Revised Manuscript Received February 11, 2002

ABSTRACT: The existence and mobility of conformational defects that could account for the α_c-relaxation in crystalline polyethylene are studied by atomistic simulation. Candidate defects are identified by an exhaustive search of conformation space. Their mobility for translation along the chain in the crystal is estimated using the Transition State Theory. Among point defects, we find a large number of candidates for the α_c-relaxation. This solution space is simplified by grouping solutions into families that yield a common minimum energy defect conformation. Dynamic pathways for defect propagation from one unit cell to the next vary substantially in energy barrier, ranging from 4 to 15 kcal/mol, in accord with experimental values of 5−22 kcal/mol. The highest mobilities (lowest energy barriers) were obtained for pathways that visit different defect conformations as they pass from one unit cell to the next. The most facile dynamic pathway for the α_c-relaxation was found to involve the cooperative rotation of two torsions within the defect while five intervening torsions remained unchanged. Finally, we propose a method for computing atomistically the activation volume associated with elastic deformation of the lattice due to defect insertion and motion. For the low barrier α_c-relaxation pathway, we obtain a contribution to the activation volume of 0.9 to 6.4 Å^3 at 0 K associated with reversible lattice distortion and a contribution of 11.1 Å^3 due to chain translation, in substantial accord with values of 19−29 Å^3 obtained at 343−424 K from dielectric α-relaxation experiments. These results indicate that relatively small, local defects in polyethylene can play a role in the dielectric α-relaxation.

Introduction

Semicrystalline polymers are attractive in a wide array of applications, due in part to their superior toughness and strength-to-weight properties compared to more traditional materials such as metals and glasses. However, despite intensive investigation over the past 3 decades, the molecular mechanisms underlying these mechanical properties are not completely understood. One reason for this is that, unlike elasticity, toughness and plasticity are determined in large part by the action of structural inhomogeneities, or defects, within the material. The ultimate strength and toughness of a material depends not only on the predominant, defect-free structure but also upon the defects themselves, which can propagate through the otherwise perfect lattice and provide a mechanism for response of the material to applied stress.

A phenomenon related to the plastic response of a semicrystalline polymer is the so-called α_c-relaxation.[1−3] Relaxations describe the time dependent response of a material to an external field and how the material returns to equilibrium after exposure to such a disturbance. The classical description of a relaxation process involves a rearrangement of the structure via passage over a barrier on the potential energy surface, in an activated process. One can think of this process as a flux of material over the energy barrier, driven by a shift in the equilibrium distribution of configurations due to application or removal of an external field.[1,4] When the external field is oscillatory and its frequency matches the rate of flux of material crossing the energy barrier, the absorption of energy by the sample appears as a "loss" peak in the frequency spectrum. Polymers exhibit multiple "loss" peaks in the frequency spectrum. By convention, the highest temperature (lowest frequency) peak is called the α-relaxation peak and is most often associated with the glass transition. The next highest temperature peak is termed the β-relaxation peak and so on.

In slightly oxidized PE, past experimental work has determined that the mechanism responsible for the dielectric α_c-relaxation occurs primarily in the crystal phase.[2,3,5] In addition, experiments on long-chain polar solutes dissolved in paraffin crystals indicate that the activation energy of the relaxation is proportional to chain length only for short chain solutes.[6,7] This evidence demonstrates that the relaxation mechanism involves motion of only a segment of the chain at a time, rather than the concerted rotation of entire chains. The conformation of such a segment, in which the atoms are necessarily displaced from their crystallographic positions in order to localize a defect within the crystal, is a " defect conformation". NMR experiments indicate that the dielectric α_c-relaxation mechanism entails the rotation of the dipole by 180° and a translation of the chain by $c/2$ in the chain direction.[8,9] Furthermore, Sayre et al. found that pressure has a significant effect on the activation parameters for the dielectric α_c-relaxation,[10] which can be quantified through an activation dilatation or an activation volume term.[11]

A renewed interest in the α_c-relaxation has occurred recently with additional two-dimensional NMR studies by Schmidt-Rohr and co-workers[12] and Porter and co-workers.[13] These studies confirm that the α_c-relaxation mechanism in PE does indeed require a 180° flip of the PE chain. Hu and Schmidt-Rohr conclude that the α_c-relaxation is a necessary (but not sufficient) condition for polymers to exhibit ultradrawability.[14]

Fröhlich first attempted to explain the dielectric loss peak in paraffins using continuum models for the chain, proposing a rigid chain flip mechanism for short chains and a smooth, elastic twist for longer chains.[15,16] Beginning in the 1960s, there were several attempts to characterize defects in crystalline polyethylene at the

10.1021/ma0118668 CCC: $22.00
Published on Web 04/27/2002

atomic level. The proposed defect conformations include "kinks",[17] "jogs",[18] "crankshaft" defects,[19−22] "smooth twists",[23−25] and short "buckled twists".[26,27] As mechanisms for the α_c-relaxation, the smooth twists and buckled twists merit special attention and are described below.

Reneker and co-workers[28−30] investigated the role of short "buckled twists" in a fixed lattice. These buckled twists are short defect conformations in a chain that returns to the surrounding crystal lattice points outside the defect region and which satisfy the boundary conditions of a crystallographic defect of helical symmetry know as a dispiration. In the case of PE, the dispiration boundary conditions are a *c*/2 displacement and a 180° rotation of one segment of the chain in the crystal relative to another; this crystallographic defect may be accomplished by any of a variety of defect conformations. In these studies, the dispiration is created by distorting a small number of repeat units from their perfect all-trans conformations to form a buckled twist. The barriers to motion of the dispiration were found by "driving" one or two preselected torsions in the buckled twist, to facilitate its translation in the chain direction. "Driving coordinates" has the limitation that the motion is restricted to a pathway in phase space prescribed by the choice of driving coordinates and may miss pathways that involve cooperative motion with the other degrees of freedom. Thus, "coordinate driving" can always locate a barrier to motion, but it cannot ensure that a true saddle point on the multidimensional energy surface has been identified. This property of coordinate driving generally leads to overestimation of the true energy barrier.

Boyd and co-workers proposed defect conformations that consist of a long "smooth" twist and an elastically distorted tail.[25] The motion of these "smooth twists" was also first described by identifying barriers to motion using a coordinate driving algorithm. These defects exhibited very low barriers to translation along the chain and led to models describing their motion through the lattice as a solitary wave.[31−33]

The importance of accurate energy barrier estimation arises when Transition State Theory (TST) is invoked to describe dynamic behavior. TST is a convenient method for describing dynamical behavior that is characterized by rare events. It approximates the rate of a dynamic process by identifying both a reactant state and a product state, and the energy barrier between these states. The rate is then given as the flux of configurations that start in the reactant state, pass over this energy barrier and terminate in the product state. In conventional TST, the energy barrier is rigorously identified as a first-order saddle point on the energy surface.[34]

More recently, Wunderlich and co-workers[35−37] investigated molecular motion in PE crystals using molecular dynamics. They describe a crystal with a large degree of molecular motion and a relatively disordered crystal state (the "condis" crystal). However, most of these molecular dynamics studies employed a united atom force field wherein the CH_2 unit is lumped into a single site. The omission of the pendant hydrogen atoms alters the symmetry and packing energy of the crystal phase as well as the heights of barriers to motion, since the latter is very sensitive to hydrogen−hydrogen interactions between neighboring chains. Sumpter et al. estimate that the rate of formation of defects varies from 2.5×10^{-9} s^{-1} for an explicit all-atom simulation to 10^{-10} s^{-1} for the united atom simulations.[36] We find that barrier heights may be lower by as much as 10 kcal/mol using a united atom force field. The relative importance of different dynamic pathways is thus altered.

In this study, we revisit the study of mechanisms responsible for the α_c-relaxation in polyethylene (PE). Our purpose in doing so is severalfold. First, it provides a simple, well-studied test case for developing a robust procedure for characterizing defect-mediated processes in crystalline polymers. Here, we outline a procedure for identifying defect conformations that accommodate a crystallographic defect of dispiration type in PE, and a method for determining the minimum energy barrier to motion of the dispiration along the PE chain. We investigate first the pathways accessible to the dispiration assuming that the defect conformation is the same in both reactant and product states, albeit displaced by one unit cell along the chain. We then investigate the multitude of pathways accessible for dispiration motion when the defect conformation is allowed to differ between reactant and product states. Second, we look at the role of volume dilatation during motion of the dispiration. Such dilatation contributes to the activation volume for the relaxation and shows up as a pressure dependence for the α_c-relaxation. Third, defect conformations of this type may have wider importance for such processes as lamellar thickening and for formation of more complicated defect structures like dislocation lines, which arise in consideration of crystal plasticity and toughness, and screw dislocations, which are important to understanding crystallization and spherulitic growth. An initial application of several components of this procedure to the study of the α_c-relaxation in polyvinylidene fluoride has been reported previously.[38]

Simulation Method

The modeling of the mechanism for the α_c-relaxation in PE requires three basic steps. First, we identify the stable conformations that are consistent with the crystallographic defect deduced from experimental observations; these serve as the possible end points for an activated process. In the case of the α_c-relaxation in PE, this defect is characterized by the axial displacement of part of the chain by a distance *c*/2, accompanied by a 180° rotation about the chain axis, as illustrated in Figure 1.[8,9] Second, given any two system configurations in which candidate defect conformations are displaced relative to one another by an integer number of unit cells, we identify a pathway across the energy surface from one configuration to the other. We compute the energy barrier to motion along this pathway by locating the first-order saddle points. Third, we quantify the local deformation of the lattice at stationary points on the potential energy surface intersected by this pathway (i.e., the minima and saddle points) and use this to compute an activation volume.

Configuration Search. For the search of candidate defect conformations, we need to specify a set of boundary conditions that define the crystallographic defect. These input conditions include the following: (a) the overall displacement spanned by the defect conformation in order to connect one stem of perfect, crystalline material to the second stem; (b) the overall twist spanned by the defect between stems; and (c) the

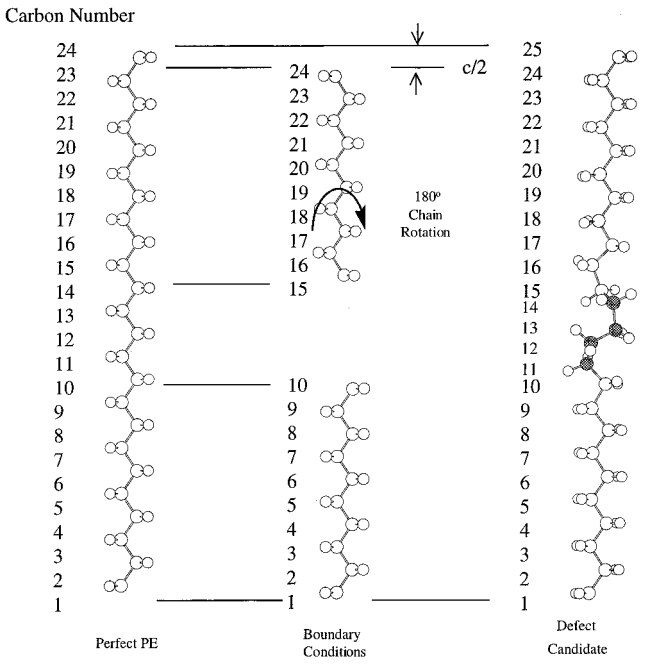

Figure 1. (Left) All-trans conformation of PE as it exists in the perfect crystal lattice. (Center) *c*/2 displacement and 180° rotation of one part of the chain to create a dispiration. (Right) Insertion of a defect conformation at carbons 11−14, which accommodates chain connectivity within the dispiration.

number of backbone atoms comprising the defect conformation. In what follows, specification of the number of backbone atoms only places an upper bound on those which may participate in the defect conformation; defect conformations involving fewer atoms are also possible. Under certain circumstances, the choice of input conditions prescribes a well-defined geometric problem. For example, given three constraints defined by the Cartesian components of a vector describing the position of one chain segment relative to the other and three constraints defined by the orientation of one segment relative to the other, one can solve for defect conformations which reconnect the segments using exactly six degrees of freedom. Assuming fixed bond lengths and bond angles, one can solve for the positions of three atoms, whose coordinates are defined by six torsion angles. Solving for the positions of a set of atoms that reconnect two segments of a polymer chain is called "rebridging".[39]

This geometric rebridging problem was recognized first by McMahon et al., who used it to identify fold conformations on a polymer crystal surface,[40] and subsequently by Go and Scheraga, who used it to study cyclic tri- and tetrapeptides.[41] The method was later incorporated into a Monte Carlo move by Dodd and co-workers[39] and used to study tetracosane and an atactic polypropylene melt. The Monte Carlo move was extended to allow rebridging to chain ends ("end-bridging") and applied to simulation of PE melts[42,43] and interlamellar domains.[44−46] This rebridging method was also used in a previous investigation of the dielectric α_c-relaxation in polyvinylidene fluoride by Carbeck and Rutledge.[38] More recently, an alternative solution to the rebridging problem was demonstrated by Wu and Deem[47] and applied to proline-containing cyclic peptides. Since this method is described thoroughly elsewhere,[38−41] we describe only some of the details here in order to convey the validity of our new "sorting" technique of

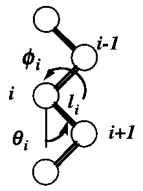

Figure 2. Definition of the internal coordinate system. l_i is the bond length, θ_i is the bond angle, and ϕ_i is the torsion angle.

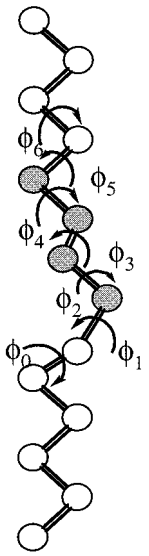

Figure 3. Torsions employed as degrees of freedom in the geometric search for stable defect conformers.. The algorithm returns the values of ϕ_{1-6} as ϕ_o is varied. White atoms remain in crystallographic positions, while gray atoms form the defect conformation.

identifying related solutions. The description follows that of Dodd and co-workers.[39]

The solution of the geometric rebridging problem requires as input a set of boundary conditions. These boundary conditions are the displacement of one segment to be rebridged from the second segment and the overall rotation of a frame of reference associated with one segment to match that of the second segment. One must also specify the number of carbons (C's) used to form the bridge. In the dielectric α_c-relaxation in PE, experimental data indicates that the boundary conditions are those prescribed by a dispiration, while the size of the dispiration and the relevant defect conformation(s) are not known. In this work, we solve for defect conformations involving only seven torsions, corresponding to four C's displaced from their crystallographic positions, which fit into a dispiration in the PE crystal. The introduction of a seventh torsional degree of freedom is handled by a one-dimensional search of analytical solutions to the rebridging problem. The question of segment size comprising the mobile defect will be addressed elsewhere.[48] These conditions uniquely specify the chain rebridging problem.

If we build a local coordinate system as shown in Figure 2 and label the torsions across the segment to be rebridged as shown in Figure 3, we can solve analytically for torsions ϕ_1 through ϕ_6 for any given value of ϕ_o. Thus, we denote ϕ_o as the "scan" torsion angle, and vary this torsion through 360° using a mesh of 10°. As we show below, this mesh size is sufficient to identify all minimum energy geometric solutions. The labeling direction for ϕ's is arbitrary and does not affect

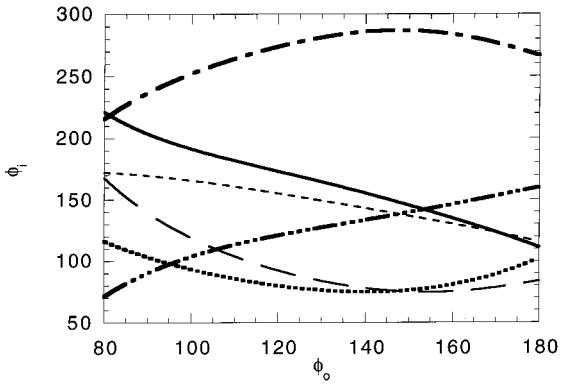

Figure 4. Example of a family, illustrating how $\{\phi_{1-6}\}$ values vary as ϕ_o is scanned from 80 to 180°: ϕ_1 (solid); ϕ_2 (dot−dash); ϕ_3 (short dash); ϕ_4 (long dash); ϕ_5 (dot−dot−dot−dash); ϕ_6 (dot).

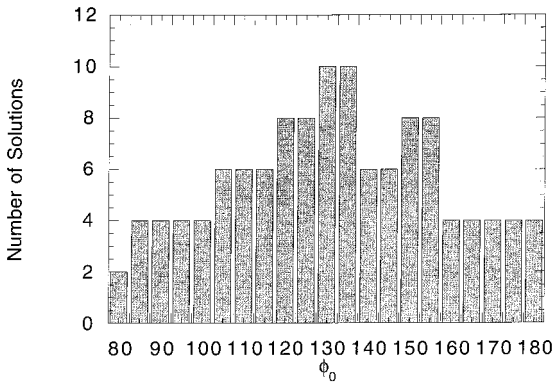

Figure 5. Histogram of the number of solutions found for various values of the scan torsion ϕ_o.

the analytical solution for the same set of boundary conditions.

The analytical solution requires finding the roots of a highly nonlinear equation denoted F_5 by Dodd and co-workers,[39] shown below.

$$F_5(\phi_1;r_5^{(1)},u_6^{(1)},\gamma_6) = [u_6^{(1)}]^T T_1 T_2 T_3 T_4 e_1 - \cos\theta_5 \quad (1)$$

Here γ_6 is the Eulerian angle that specifies the orientation of unit bond vector u_7 about an axis specified along the preceding unit bond vector. The T_i's represent rotation matrices in the *xy* and *yz* planes converting coordinates from local coordinates centered on atom $i + 1$ to a coordinate system centered on atom i, and $e_1 = (1\ 0\ 0)^T$. The term θ_5 represents bond angle 5 (Figures 2 and 3). Equation F_5 has a series of "branches" due to multiple solutions for the set of torsions $\{\phi_1,\phi_2,\phi_3,\phi_4,\phi_5,\phi_6\}$ (henceforth abbreviated $\{\phi_{1-6}\}$) for any given value of ϕ_o. Thus, each root of F_5 results in a unique set $\{\phi_{1-6}\}$ of torsions that reconnect the polymer chain, for the boundary conditions specified, with fixed bond lengths and angles. Each of these roots of F_5 comprises the set of six torsion angles $\{\phi_{1-6}\}$, the values of which can be followed as we vary ϕ_o, the scan torsion. This leads to a mathematically continuous set of roots $\{\phi_{1-6}\}$ which we designate a "family". For different values of ϕ_o, we find regions with no families, multiple families, or a single family. A family can be formally defined as a set of $\{\phi_{1-6}\}$'s where for two values of the scan torsion, ϕ_{oA} and ϕ_{oC} with solutions $\{\phi_{1-6}\}_A$ and $\{\phi_{1-6}\}_C$ respectively, we find either $\phi_{i,A} < \phi_{i,B} < \phi_{i,C}$ or $-\phi_{i,A} < -\phi_{i,B} < -\phi_{i,C}$ for all ϕ_i (depending on whether it is an increasing or decreasing function of ϕ_o) and any ϕ_{oB} such that $\phi_{oA} < \phi_{oB} < \phi_{oC}$. This holds for each branch of F_5 . Figure 4 illustrates the variation in values for ϕ_1 through ϕ_6 in one such family as ϕ_o is varied from 80 to 180°, the range over which this family exists. Since F_5 is a multivalued mapping, i.e., a relation that has multiple roots $\{\phi_{1-6}\}$ for any given set of boundary conditions and choice of ϕ_o, we can identify a family associated with each root. For values of ϕ_o that are sufficiently similar, one finds roots of F_5 that belong to a common group of families. However, the number of roots varies for dissimilar values of ϕ_o, resulting in families that exist only over a limited range of ϕ_o's. Figure 5 shows the number of families vs the scan torsion ϕ_o for the boundary conditions required by the α_c-relaxation in PE. Each of these families has a similar appearance to the one in Figure 4, with the only difference being the range of scan torsion values for which a root of F_5 exists and belongs to that family.

Grouping solutions to the rebridging problem by families serves several purposes. First, the continuity of $\{\phi_{1-6}\}$ within a single family ensures that all solutions can be found by refining the mesh in ϕ_o sufficiently. Next, we can use the family groupings to sort the solutions and search for minimum energy configurations. Upon minimization, roots belonging to a single family will settle into either the same or different minimum energy configurations. For entire sections of the family which settle into the same energy minimum, we retain only the minimum energy conformation and reduce the number of "distinct" defect conformations accordingly. A family in which consecutive ranges of ϕ_o settle into different energy minima defines an adiabatic pathway connecting two defect conformations following a trajectory prescribed by fixed bond lengths and angles. Using this method of sorting, one can show that the algorithms of Reneker and co-workers for finding and "driving" defects along the chain using one driver angle[27] is analogous to solving the geometric problem for one root, and then "driving" this solution by varying a single torsion (ϕ_o in our notation) in small increments while minimizing the remaining degrees of freedom for each new value of ϕ_o. The result is that motion of the defect along the chain corresponds to traversing the set of roots comprising a single family.

The geometric search algorithm of Dodd et al.,[39] described briefly above, was applied to single atomistic chains of PE 25 C's in length. The defect conformations include up to four C's. The resulting geometric solutions were then sorted into families by identifying the sets of torsions related to one another as we scanned over ϕ_o. We then placed these candidate defects into a perfect lattice of $2 \times 3 \times 12$ ($a \times b \times c$) unit cells, containing 11 neighboring chains of length 24 C's (i.e., the interstitial defect accounts for one extra carbon in the candidate conformation) in the all-trans conformation. The constraints of fixed bond lengths and bond angles on the chain containing the defect conformation were then relaxed and the energy was minimized in a Cartesian coordinate system, holding the positions of the first two and last two repeat units fixed. Periodic boundary conditions were used with a cutoff of 6.5 Å for nonbonded interactions. Energy minimizations were carried out using the variable metric method of Broyden, Fletcher, Goldfarb, and Shanno.[49] All energy calculations used the variation of the Sorensen force field[50] described by Martonak, Paul, and Binder,[51] since the latter eliminates the discontinuity in the vicinal bend−

bend potential which causes convergence problems for the saddle point algorithm described below.

Saddle Point Search. To identify saddle points, we used the conjugate peak refinement algorithm (CPR).[52] CPR estimates a lowest energy pathway between two minima, by convention designated as "reactant" and "product" states. However, the results are insensitive as to which minimum is designated as "reactant" or "product". The algorithm continually refines a pathway between these two minima, *i* and *j*, starting with a straight line $\mathbf{s} = \mathbf{x}_j - \mathbf{x}_i$ in configuration space. The energy is first maximized subject to the constraint that the configuration lies on the line **s**. The algorithm then minimizes the energy in the $(N-1)$-dimensional space conjugate to the pathway, **s**, using the derivatives of the energy and Beale's method of generating a basis set. This new point, now maximized in one dimension and minimized in $N-1$ dimensions, serves as the first estimate of the saddle point. The algorithm then searches the two segments connecting the original energy wells *i* and *j* to this new point, *k*, repeating the procedure above for each segment. This is continued with additional points added to the pathway as the curvature of the surface dictates. The algorithm terminates when all intermediate maxima on the pathway are identified as saddle points. Thus, the CPR method can determine paths with multiple saddle points and many degrees of freedom.

The CPR algorithm requires only the energy function and first derivatives. The points on the potential energy surface identified as saddles by the CPR algorithm were confirmed to be true first-order saddle points by diagonalizing the Hessian matrix of second derivatives using the Householder method of tridiagonalization followed by the QL diagonalization routine.[49] Given the reaction path identified by CPR, the intrinsic reaction coordinate (IRC)[53] and all intermediate minima can be found by minimization of energy starting from each of the saddle points found. The IRC represents a pathway of infinitesimal steps along the direction of the maximum local force or gradient of energy, in mass-weighted coordinates. We use a conjugate gradient minimization path in Cartesian coordinates as an approximation to the IRC throughout this investigation.

A useful property of CPR is that it locates the highest energy saddle point separating two states first, and then identifies other, subsidiary saddle points in subsequent iterations. The algorithm accomplishes this task by continuously reevaluating the energy path connecting reactant and product and refining the highest energy maximum along the path at that iteration. When this refinement first produces a saddle point, any additional saddle points found will necessarily be lower, since every other current point on the pathway is already lower in energy than this saddle. Further refinement (i.e., minimization conjugate to the reaction coordinate direction) only serves to lower the energy of these other points further and increases the barrier height differential between the maximum saddle and these other, lower saddle points. As a matter of computational efficiency, this property of CPR can be used to speed up the TST calculations by approximating the reaction pathway as a smooth curve passing though the first (i.e., highest energy) saddle point identified. More complicated pathways may be obtained upon further refinement. For rare event processes like the α_c-relaxation in PE, we find it useful to approximate the dynamics within the crystal by examining only the "slowest" step in the process, commonly known as the rate-limiting step (RLS). The RLS in a series of reactions can be defined as that with the highest activation barrier.[54] The RLS in this paper is taken to be the activation barrier between the highest saddle point and the reactant. This approximation holds provided the intermediate points along the reaction path have energies approximately the same as or higher than the reactant.[55] If the intermediate points along the IRC have energies much lower than the reactant, then the highest energy barrier may be underestimated using this procedure. We assume that our exhaustive search of phase space in the geometric problem identifies the lowest energy defect conformations, and thus the energies along the IRC should be at least as high as that required to form the reactant.

The IRC represents a 1-D curvilinear reaction coordinate in $3N$ dimensional space. In this work, $N = 51$, corresponding to the central 17 C's of the chain containing the defect conformation plus their substituent H's. To characterize positions along the reaction coordinate, we compute the fractional arc length traversed along this curvilinear path. We use a piecewise linear approximation for the arc length. For any two neighboring points i and i-1 along the reaction coordinate we have

$$s_i = \sqrt{\sum_{k=1}^{N_{\text{atoms}}} (r_i - r_{i-1})_k \cdot (r_i - r_{i-1})_k} \tag{2}$$

and the cumulative sum up to point k is given by

$$\hat{s}_k = \sum_{i=1}^{k \le N} s_i \tag{3}$$

Then the fractional arc length is

$$\xi_i = \frac{\hat{s}_i}{\hat{s}_N} \tag{4}$$

This provides a meaningful representation of the reaction coordinate profile for defect motion with realistic curvature of the potential energy surface throughout. This also means the curvature of the pathway is accurate near the saddle points, which can be important for estimating barrier recrossings and tunneling.

For purposes of comparison, we have also characterized position along the reaction coordinate using the method of Reneker et al.[27] They defined the position of the defect by an "average atom number", $\bar{n}$:

$$\bar{n} = A\sum_n n(\delta_n - \delta_{n-1}) \tag{5}$$

where δ_i is the difference in the *z*-coordinate (along the chain axis direction) between a carbon in the defect conformation and the corresponding carbon in the all-trans conformation of a chain in the perfect crystal. $A^{-1} = \sum_n(\delta_n - \delta_{n-1}) = c/2$ is the total translational mismatch along the chain axis associated with the defect. In similar fashion, Reneker et al. also defined the variance of the defect as

$$\sigma_n = A\sum_n (n - \bar{n})^2(\delta_n - \delta_{n-1}) \tag{6}$$

The variance offers a measure of the size of the defect.

For pathways identified using the coordinate driving method, eq 5 provides a useful measure of the "average" defect position. In general, however, a defect propagating along a curvilinear reaction coordinate may appear to backtrack if measured along any one of the Cartesian axes. For this reason, we favor the piecewise linear arc length metric.

Activation Volume. Insertion of a defect an otherwise perfect crystal results in an increase ($d\Psi$) in the free energy of the crystal. In general, this increase in free energy leads to deformation of the crystal, which is resisted by the elasticity of the crystalline surroundings:

$$d\Psi = V\boldsymbol{\sigma}^T\epsilon = \frac{1}{2}V\epsilon^T\mathbf{C}\epsilon \tag{7}$$

V is the volume of the reference crystal, $\mathbf{C}$ is the elastic stiffness tensor of the crystal, σ is the stress that arises from an imposed strain ϵ (Voigt notation). For a macroscopic crystal, the strain induced by a single defect is exceedingly small but finite. For example, if V is the volume of the crystal and δV is the change in volume due to defect insertion, then the bulk strain $\delta V/V$ approaches zero for $V \gg \delta V$, even while δV remains finite. To evaluate the stress dependence of the α_c-relaxation, we define an activation volume tensor ($V\epsilon$) for the crystallographic defect due to deformation of the lattice associated with insertion of the defect. In general, insertion of a defect into a crystal lattice results in both dilatation (or contraction) and shear of the crystal. This activation volume tensor is a generalization of the activation volume δV associated with defect insertion into the crystal lattice. We assume that the energy of defect insertion, and hence the activation volume tensor, is characteristic of the defect and is independent of the size of the perfect crystal lattice into which it is inserted. According to eq 7, as we consider larger reference volumes of crystal, the true strain observed must be smaller to maintain a constant $d\Psi$. Using the site of the defect as a reference point, chains within a local region surrounding the defect may be significantly displaced relative to one another, resulting in an increase in energy. Chains that are distant from the site of the defect are displaced equally from their corresponding positions in the perfect crystal but are not displaced relative to one another and hence do not contribute any additional energy. This is illustrated schematically in Figure 6. The total activation volume is the work of lattice deformation plus any irreversible work associated with displacement of the chain (e.g., due to passage of the defect). To account for the work of lattice deformation, we compute an activation volume tensor as follows.

An undeformed portion of the crystal lattice is described by a matrix $\mathbf{h}_0 = [n\mathbf{a}, m\mathbf{b}, p\mathbf{c}]$, where $\mathbf{a}$, $\mathbf{b}$, and $\mathbf{c}$ are the unit cell vectors and n, m, and p are integers defining a supercell comprised of $n \times m \times p$ such unit cells. After insertion of a point defect in this supercell, $\mathbf{h}_0$ is deformed to some new matrix $\mathbf{h}$. The strain accompanying this change in the supercell can be computed as[56]

$$\epsilon = \frac{1}{2}(\boldsymbol{h}_0^{T,-1}\mathbf{G}\mathbf{h}_0^{-1} - 1) \tag{8}$$

where $\mathbf{G} = (\mathbf{h}^T\mathbf{h})$. For ϵ sufficiently small, the activation volume tensor is $V_0\epsilon$. The scalar activation volume ΔV is V_0 Tr(ϵ).V_0 is the volume of the undeformed supercell and Tr indicates the trace. Our simulations indicate that simulations of $2 \times 4 \times 12$ unit cells are sufficient to capture ΔV. This simulation cell size was tested by performing additional calculations with $3 \times 4 \times 12$ and $3 \times 5 \times 12$ unit cell simulations which change the value of ΔV obtained by less than 2%.

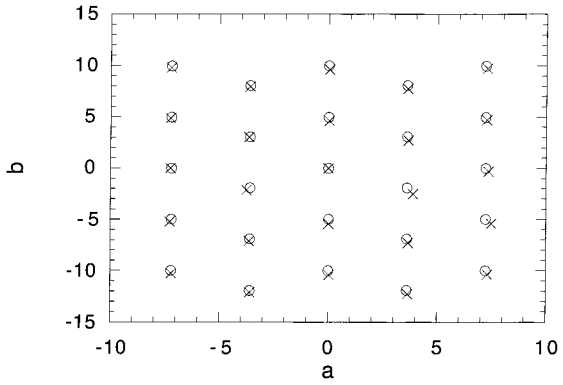

Figure 6. Diagram illustrating the displacement of the centers of mass of chains in the crystal as a result of insertion of a defect-containing chain. The view is down the *c*-axis of the crystal. The ○'s represent chain positions in the perfect PE lattice while the ×'s represent chain positions after defect insertion. The axis labels correspond to crystallographic directions *a* (along the *x*-axis) and *b* (along the *y*-axis). The units are in Å. The chain containing the defect is located at (0,0). The displacements are magnified by a factor of 2 for clarity.

To compute the matrix $\mathbf{h}$, we placed the conformations found from the minimization step during the configuration search and the saddle point search in a crystal lattice containing $2 \times 4 \times 12$ unit cells, i.e., 15 chains of length C24 in the all-trans conformation surrounding one chain containing the defect. The energy of this cell was minimized while holding all the chain conformations fixed, but allowing all the chain parameters (i.e., the chain setting angle, chain center of mass coordinates, etc.) and the unit cell dimensions to vary (i.e., zero applied pressure). Periodic boundary conditions and Ewald summation[57] were used to account for long-range interactions. For the activation volume associated with defect formation, we take $\mathbf{h}_o$ corresponding to the perfect crystal dimensions and $\mathbf{h}$ given by the supercell dimensions after minimization with the stable defect in the central chain. For the activation volume associated with defect motion, we take $\mathbf{h}_o$ corresponding to the supercell dimensions after minimization with the stable defect and $\mathbf{h}$ given by the supercell dimensions after minimization at the saddle point configuration. To this, we add the volume swept out by the chain translation, computed as the cross-sectional area of the chain (taken to be $^1/_2$ the *ab* facet of the PE unit cell) times the *c*/2 displacement. The activation volume can be obtained from experimental measurements of the pressure dependence of relaxation frequency, *f*, using the Arrhenius expression

$$\ln f = \left(\ln \nu_o + \frac{\Delta U}{RT}\right) - \frac{P\Delta V}{RT} \tag{9}$$

where ν_o is the attempt frequency for molecular motion over the energy barrier, ΔU is the potential barrier, and P is the hydrostatic pressure.

Results

Configuration Search. Applying the configuration search algorithm to the problem of identifying defect

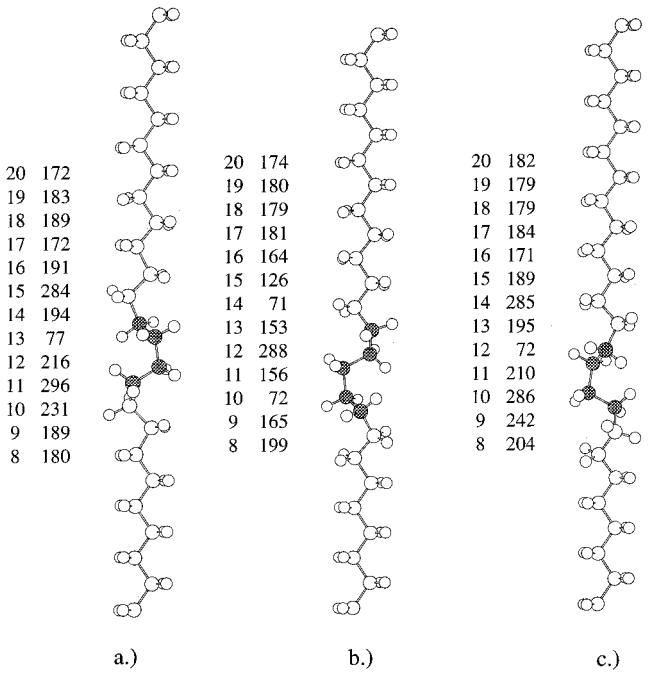

Figure 7. Three defect conformations having the lowest energy of formation (see text for details). Values of numbered torsions that deviate from trans are indicated to the left of each conformer. (a) Conformer 1: $E_{form} = 10.78$ kcal/mol. (b) Conformer 2: $E_{form} = 11.03$ kcal/mol. (c) Conformer 3: $E_{form} = 11.08$ kcal/mol.

conformations up to four carbons long for the PE dispiration produces a total of 10 unique families over the domain $\phi_o = [0, 180°)$. Symmetry in the PE crystal results in a mirror image solution set over the domain [180, 360°). We found that a driver torsion mesh of 10° was sufficient to identify all the families associated with the dispiration boundary conditions, since further reductions in mesh size did not identify any new families. The total number of families for the entire domain of [0°, 360°) is actually 16, since four families are common to both the [0°, 180°) and [180°, 360°) domains. The conformations belonging to these families, corresponding to roots of F_5, exhibit energies on the order of 80 kcal/mol. Upon insertion of these conformations into the perfect PE lattice and minimizing with respect to all 51 degrees of freedom, as described above, we obtain a total of 50 unique defect conformations, with energies ranging from 11 to 25 kcal/mol. Henceforth, we limit our discussion to these 50 defect conformations corresponding to energy minima within the lattice. Our method identifies several of the conformations found previously by Reneker and co-workers[27] to within a few degrees, albeit with different energies due to differences in the force fields used. The three lowest energy defect conformations are shown in Figure 7. A histogram of formation energies for the 50 stable defect conformations identified for PE is shown in Figure 8.

Reaction Pathway. The next step in the defect characterization process was to determine barriers to motion for low energy conformations of the defect found using the procedure described above. The adiabatic reaction pathway was found by translating the initial structure by one unit cell (i.e., one repeat unit) in the *c*-direction and then applying the CPR saddle point search.[52] We initially assumed that the defect visits the same defect conformation (call it "conformation A") as it passes through each unit cell during its motion along

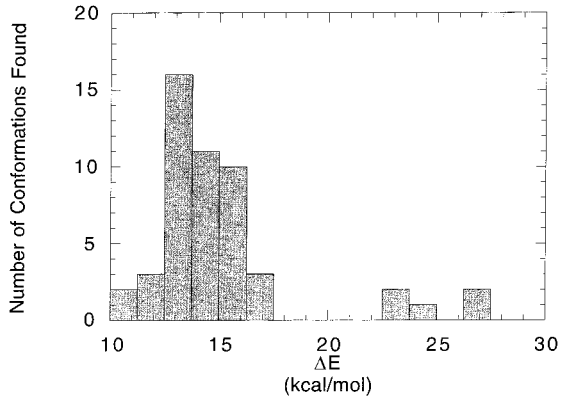

Figure 8. Distribution of defect formation energies (kcal/mol) for the dispiration in PE.

the chain. We designate this an "A-to-A" mechanism for the α_c-relaxation. Of course, the conformations of the defect at intermediate points along the reaction pathway may vary.

The results for the A-to-A mechanisms associated with the two lowest energy defect conformations (conformers 1 and 2 in Figure 7) are summarized in Figures 9 and 10. In each case, the pathway is plotted vs fractional arc length, given by eqs 2−4. These two pathways were confined to 17 C's plus their substituent H's, as described earlier. In Figure 9a, the barrier to defect motion is 14.5 kcal/mol. Conformations taken by the defect at several points along the pathway are shown in Figure 9b. These intermediate conformations have additional energy due to larger torsional and intermolecular interaction energies when compared to the stable defect conformations that comprise the end points of the reaction path. The motion is accomplished via several local minima; the low energy minimum located halfway along the reaction path corresponds to a defect conformation displaced by one-half unit cell along the chain in the *c*-direction. This intermediate stable defect conformation has the same torsional sequence as the original reactant, simply beginning 1 C further down the chain. Thus, this conformation is approximately equivalent to the original reactant but displaced by a *c*/2 translation and 180° rotation. Similarly, the barrier to defect motion starting from the second candidate defect conformation, Figure 10a, is comparable at 14.0 kcal/mol, with relevant conformations of the defect as it traverses the pathway shown in Figure 10b. Once again, an intermediate conformation was found to be approximately equivalent to the reactant with a *c*/2 translation and 180° rotation.[58]

In Figures 9c and 10c, we plot the position and size of the dispiration as defined by eqs 5 and 6 vs the reaction pathway (eq 4) for the two candidate mechanisms. These plots illustrate two fairly general characteristics of the defects reported here. First, the preferred pathway is not limited to monotonic progression in the *z*-direction but involves displacements that move the "average *z* position" of the defect both forward and backward along the chain. Second, the size of the defect is relatively insensitive to position and close to the maximum size allowed by the calculation (i.e., 17 carbons). This could be taken as indication that the calculations presented here artificially limit the size of the defect and that lower energies could be obtained by allowing the defects to spread over a larger section of the chain. Preliminary calculations, however, indicate

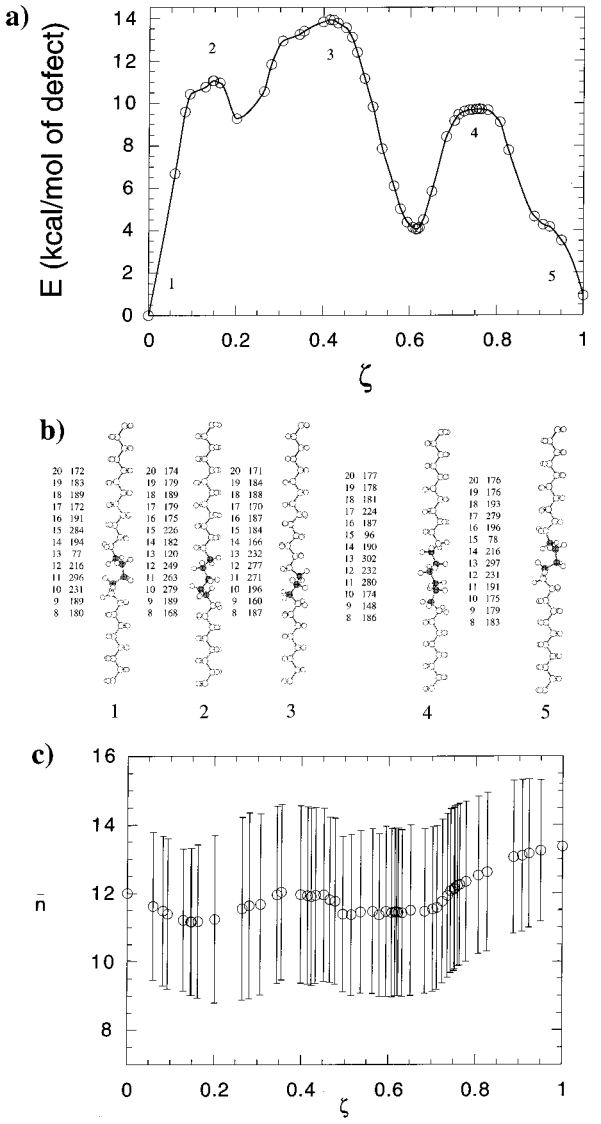

Figure 9. Results for movement of conformer 1 by a distance of one unit cell along the chain: (a) adiabatic reaction pathway, $\zeta = 0$ and 1, corresponding to equivalent positions in successive unit cells; (b) conformations of the defect at several points along the adiabatic reaction pathway, indicated in part a, where values of numbered torsions which deviate from trans are indicated to the left of each conformer; (c) position ($\bar{n}$, open symbols) and size (bars indicate $\pm\sigma_n$) of the defect at several points along the adiabatic reaction pathway, computed using the method of Reneker et al.[27]

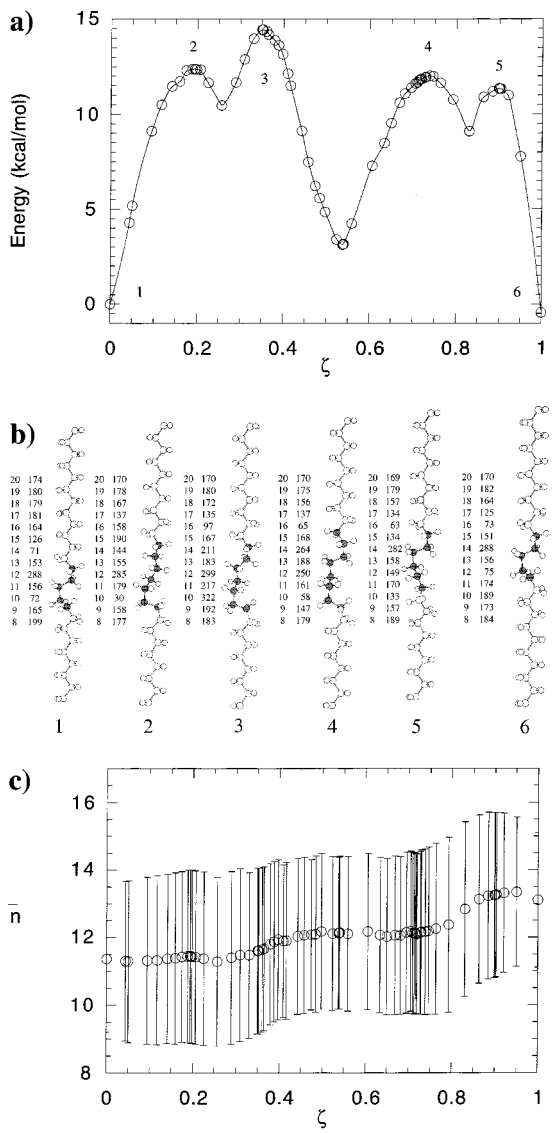

Figure 10. Results for movement of conformer 2 by a distance of one unit cell along the chain: (a) adiabatic reaction pathway, $\zeta = 0$ and 1, corresponding to equivalent positions in successive unit cells; (b) conformations of the defect at several points along the adiabatic reaction pathway, indicated in part a, where values of numbered torsions which deviate from trans are indicated to the left of each conformer; (c) position ($\bar{n}$, open symbols) and size (bars indicate $\pm\sigma_n$) of the defect at several points along the adiabatic reaction pathway, computed using the method of Reneker et al.[27]

that this is not the case. Defects of larger size will be the subject of a subsequent report.

Finally, we examined the RLS to motion through the lattice for A-to-A mechanisms based on each of the 50 defect conformations we found. Figure 11 shows a plot of the RLS barrier height ($E_{\text{saddle}} - E_{\text{form}}$) for all the A-to-A mechanisms vs the formation energy (E_{form}) for the corresponding stable defect conformations. Since the relative importance of different pathways depends on both the concentration of defects in the reactant state (proportional to $\exp(-\beta E_{\text{form}})$ at equilibrium) and the rate of barrier crossing (proportional to $\exp(-\beta(E_{\text{saddle}} - E_{\text{form}}))$), knowledge of E_{saddle} is useful for screening different pathways. All of the 50 mechanisms found have saddle point energies (relative to the defect-free crystal) on the order of 20−35 kcal/mol for motion of the defect along the chain. This is higher than expected from experimental data, making them unlikely candidates for the dielectric α-relaxation. Each of these pathways assumed that the defect propagates through the crystal in a self-similar fashion (an "A-to-A" mechanism). It is possible that lower barriers to motion may be realized by allowing the defect to visit different defect conformations (an "A-to-B" mechanism) as the defect passes through each unit cell. This possibility greatly expands the number of pathways available to move a defect through the lattice, and leads to a combinatorially large number of possible mechanisms for the α_c-relaxation. An appropriate Monte Carlo method to sample the distribution of such mechanisms will be the subject of a subsequent report. Here, we report results for a representative subset of such A-to-B mechanisms, to illustrate their characteristics.

To facilitate this preliminary evaluation, we again invoke the approximation that the highest energy saddle

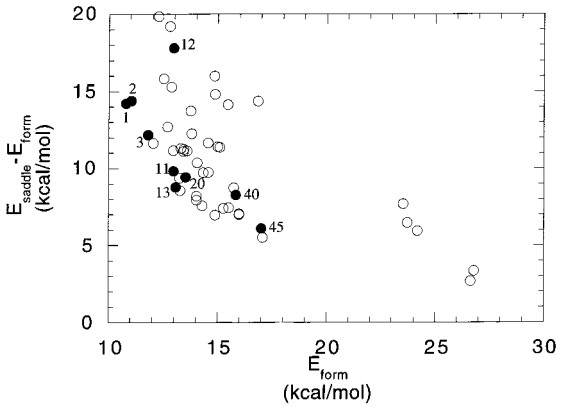

Figure 11. RLS energy barriers for A-to-A type mechanisms plotted vs the energy of formation of the corresponding defect conformations. The solid circles represent defect conformations singled out for discussion in the text. The open circles designate mechanisms associated with other defect conformations found during the geometric search. The numbers are used to label particular defects discussed in the text, and are ordered by increasing energy of formation.

point provides an adequate description of the RLS. Unlike A-to-A mechanisms, which by construction ensure a complete description of the pathway required to move the defect by one unit cell, A-to-B mechanisms may provide only a partial description of the pathway necessary to propagate the defect along the chain; a subsequent B-to-A mechanism, or something similar, may be needed to complete the description. For example, B may be a contracted form of A, or pathways out of B may convert immediately back into A in the original unit cell, without effecting translation along the chain. These latter two cases may be sufficient to account for rapid 180° rotations of a local section of the chain but do not necessarily provide a mechanism for motion of the defect down the chain axis, as would be required for the mechanical α_c-relaxation.

Examination of a subset of A-to-B mechanisms identified several pathways with lower saddle point energies than for any A-to-A mechanism. Low energy saddle points were found for pathways from conformer 11 (E_{form} = 12.97 kcal/mol) to conformer 20 (E_{form} = 13.17 kcal/mol), as well as conformer 12 (E_{form} = 12.99 kcal/mol) to conformer 13 (E_{form} = 13.07 kcal/mol). Assignments of torsional sequences in the important conformations for each mechanism are shown in Table 1. As a point of comparison, the torsional sequences for one A-to-A mechanism (conformer 12) is also shown in Table 1. The lowest energy structures found using the method above are those with the G or G′ bonds separated by one or more T bonds.

Closer examination of Table 1 reveals that the pathway from conformer 11 to conformer 20 is relatively simple and requires only the alteration of two torsions, with the remainder of the defect conformation unchanged. Bonds 10 and 16 in both stable conformations are collinear. This rotation about two collinear torsions is similar in spirit to the simple "crankshaft" models.[19−22]

Several other paths with low barriers for their RLS were found; these typically either end or begin in a relatively high energy defect conformation. A transition from conformer 3 (E_{form} = 11.08 kcal/mol) to conformer 45 (E_{form} = 15.98 kcal/mol) has a low barrier to motion but conformer 45 is very high in energy. This pathway is illustrated in Table 2. Two other paths (40, 45) and (20, 45), which were also found to have low energy barriers for their RLS's, are shown in Table 2.

Mechanisms (3, 45), (40, 45), and (25, 45) are especially interesting since they share a common saddle point configuration, but the pathway away from the saddle is different in each case. This indicates that several different mechanisms may share portions of their IRC but still result in different overall changes in the minimum energy defect conformations (torsional sequences) as translation along the chain occurs. This behavior suggests that estimating the barrier based upon "ad hoc" assumptions such as the curvature of the potential energy suface near the minima or saddle points is unlikely to identify all relevant mechanisms.[59] In general, these other mechanisms are not as simple as the crankshaft motion postulated earlier

These results agree substantially with the earlier study of Reneker and co-workers.[27] They also report mechanisms which are both A-to-A and A-to-B in character, although the distinction in their study is less apparent. They found a low barrier process of about 4 kcal/mol for movement of the defect along an A-to-B pathway. The lowest barrier reported in that work for A-to-A mechanisms is about 9.4 kcal/mol, or double the A-to-B energy barrier. Using the force field developed by Sorensen and co-workers,[50] the barrier heights we find are uniformly higher than those reported by Reneker et al. but show similar advantages for A-to-B mechanisms.

Unlike A-to-A mechanisms, which always translate the defect by one complete unit cell, A-to-B type mechanisms translate the defect by different amounts depending upon the particular A−B pair examined. Some

Table 1. Defect Conformations for Mechanisms Discussed in the Text

torsion	conformer 11	saddle point	conformer 20	conformer 12	saddle point	conformer 13	conformer 12	saddle point	conformer 12
8	T	T	T	T	T	T	T	T	T
9	T	T	T	T	T	T	T	TG	T
10	G	T	T	G	TG	T	G	TG	T
11	T	TG	T	T	T	T	T	TG	T
12	G	G	G	G′	G′	G′	G′	TG	G
13	T	T	T	T	TG′	T	T	T	T
14	G′	G′	G′	G	G′	G′	G	T	G′
15	T	T	TG′	T	T	T	T	T	T
16	G	G	G′	T	T	G	T	G	G
17	T	T	T	T	T	T	T	T	T
18	T	T	T	T	T	T	T	T	T
E (kcal/mol)	12.97	17.90	13.17	12.99	17.65	13.07	12.99	30.78	12.99

[a] T denotes a trans state (0 ± 30°), while G and G′ denote gauche states (120 ± 30 and −120 ± 30°, respectively). Torsions that do not fall within one of these domains are designated by two letters (e.g., "TG"), indicating the two states between which the torsion lies, with the first letter indicating the closer state.

Table 2. Defect Conformations for Additional Mechanisms Discussed in the Text[a]

torsion	conformer 3	saddle point	conformer 45	conformer 20	saddle point	conformer 45	conformer 40	saddle point	conformer 45
8	T	T	T	T	T	T	T	T	T
9	T	T	T	T	T	T	T	T	T
10	G	TG	T	G	TG	T	GT	TG	T
11	T	T	T	T	T	T	G	T	T
12	G′	G′	G′	G′	G′	G′	T	G′	G′
13	T	TG′	G′T	TG′	TG′	G′T	G′	TG′	G′T
14	G	G′	G′	G′	G′	G′	T	G′	G′
15	TG	T	T	T	T	T	T	T	T
16	T	T	T	T	T	T	T	T	T
17	T	T	T	T	T	T	T	T	T
18	T	T	T	T	T	T	T	T	T
E (kcal/mol)	11.08	17.65	15.98	14.05	17.65	15.98	13.21	17.65	15.98

[a] T denotes a trans state (0 ± 30°), while G and G′ denote gauche states (+120 ± 30 and −120 ± 30°, respectively). Torsions that do not fall within one of these domains are designated by two letters (e.g., "TG"), indicating the two states between which the torsion lies, with the first letter indicating the closer state.

Table 3. Activation Strain Tensor Components for Two Mechanisms with Low Energy Barriers

process	ϵ_{11}	ϵ_{22}	ϵ_{33}	ϵ_{23}	ϵ_{13}	ϵ_{12}	Δv_p, activation dilatation, Å^3
conformer 20 to saddle point	0.0014	−0.0013	0.000006	−0.0005	0.0013	0.0013	0.90
conformer 11 to saddle point	−0.00045	0.001 17	0.000000	−0.0021	0.0013	0.000 63	6.37

A-to-B type mechanisms change both the size and position of the defect conformation, such as is the case for transition from conformer 11 to 20 shown in Table 1. This mechanism results in an increase in $\bar{n}$ (see eq 5) from 12.4 to 13.6. Thus, the position of the defect moves by only 1.2 C's instead of 2 C's, as would be the case in a pure "A-to-A" mechanism. This low barrier "partial" defect translation also is in agreement with the earlier Reneker study[27] which reported a low barrier process with a net translation of the defect by approximately 1.7. Other A-to-B transitions translate the defect farther along the chain, such as the case for transition from conformer 12 to 13. In this case, $\bar{n}$ changes by 1.8. The torsional sequence shown in Table 1 for the transition from conformer 12 to 13 also appears to advance along the chain with no contraction as in the transition from conformer 11 to 20. Thus, we find A-to-B mechanisms with low energy barriers that translate the defect by varying amounts along the chain.

The results in Tables 1 and 2 suggest that the explanation of chain transport within crystal lamellae by motion of point defects is quite complicated. Most importantly, it shows clearly that the process is almost certainly not the result of a single mechanism but rather a complex process involving repeated A-to-B mechanisms and several defect conformations.

Activation Volume Results

To compute activation volumes for the defect hopping processes, we performed variable volume simulations as described above in the Simulation Method section. We found the activation strains shown in Table 3 for the low barrier energy mechanism described above (i.e., for the "A-to-B" mechanism involving conformers 11 and 20). The activation strains are also given in Table 3 for the mechanism from conformer 20 to 11. We find the activation strain has a directional dependence, with larger strain required for the motion from conformer 11 to 20 than from conformer 20 back to 11. The volume swept out by the defect during translation of the chain is 11.1 Å^3 at 100 °C. Sayre et al. report activation volumes of 12−18 cm^3/mol at temperatures ranging from 70 to 151 °C,[10] or 19.9−29.9 Å^3 per activated event (assuming numbers are reported per mole of activated events). These results suggest that work associated with displacement of the chain during defect motion constitutes the main part of the activation volume but that elastic deformation of the lattice can be as much as 25% of the total activation volume for defect motion in some cases.

Conclusions

A computational evaluation of the atomic scale mechanisms responsible for the α_c-relaxation in PE has been presented. These mechanisms begin and end with defect conformations that are stable and consistent with the crystallographic defect of dispiration type, which has been deduced from experimental data. The defect conformations considered in this work are relatively small, involving four or fewer carbons displaced from their crystallographic positions. We find that even for a relatively simple and well-defined case like the PE α_c-relaxation, a large number of mechanisms may be involved. While the simplest mechanisms to identify are of the A-to-A type, wherein the same defect conformation is visited in each unit cell as the defect moves along the chain, the more numerous and lower energy mechanisms are of the A-to-B type, wherein different defect conformations are visited as the defect moves down the chain. However, care must be taken with the latter class of mechanisms to ensure that long range motion is actually obtained, rather than simple rearrangement of bonds or a flip-flop motion between two isolated defect conformations connected by a low energy barrier. In general, low energy defect conformations exhibit high barriers to propagation, whereas high energy defect conformations exhibit lower barriers to propagation. We consider it most likely that the dominant mechanisms are those involving defect conformations of moderate energy (12−14 kcal/mol), which propagate with energy barriers on the order of 10−15 kcal/mol.

References and Notes

(1) McCrum, N. G.; Read, B. E.; Williams, G. *Anelastic and Dielectric Effects in Polymeric Solids*; John Wiley and Sons: New York, 1967.
(2) Boyd, R. H. *Polymer* **1985**, *26*, 323.
(3) Boyd, R. H. *Polymer* **1985**, *26*, 1123.

(4) DeBatist, R. *Internal Friction of Structural Defects in Crystalline Solids*; North-Holland: New York, 1972.
(5) Ashcraft, C. R.; Boyd, R. H. *J. Polym. Sci. Polym. Phys. Ed.* **1976**, *14* (12), 2153.
(6) Meakins, R. J. *Trans. Faraday Soc.* **1959**, *55*, 1694.
(7) Meakins, R. J. Mechanisms of Dielectric Absorption in Solids. In *Progress in Dielectrics*; Birks, J. B., Hart, J., Eds.; Heywood and Co.: London, U.K., 1961; Vol. 3.
(8) Olf, H. G.; Peterlin, A. *J. Polym. Sci. A-2* **1970**, *8*, 753.
(9) Olf, H. G.; Peterlin, A. *J. Polym. Sci. A-2* **1970**, *8*, 771.
(10) Sayre, J. A.; Swanson, S. R.; Boyd, R. H. *J. Polym. Sci. Polym. Phys. Edn.* **1978**, *16*, 1739.
(11) Argon, A. S. Mechanical Properties of Single Phase Crystalline Media In *Physical Metallurgy*, 4th ed.; Cahn, R. W., Haasen, P., Eds.; North-Holland: New York, 1996.
(12) Hu, W. G.; Boeffel, C.; Schmidt-Rohr, K. *Macromolecules* **1999**, *32*, *2* (5), 1611.
(13) Kanamoto, T.; Tsuruta, A.; Tanaka, K.; Takeda, M.; Porter, R. S. *Macromolecules* **1988**, *21*, 470.
(14) Hu, W. G.; Schmidt-Rohr, K. *Acta Polym.* **1999**, *50*, 271.
(15) Fröhlich, H. *Proc. Phys. Soc. London* **1942**, *54*, 422.
(16) Fröhlich, H. *Theory of Dielectrics*, 2nd ed.; Oxford University Press: Oxford, U.K., 1958.
(17) Pechold, W.; Blasenbrey, S.; Woerner, S. *Kolloid, Z.* **1963**, *189*, 14.
(18) Predecki , P.; Statton, W. O. *J. Appl. Phys.* **1967**, *38*, 4140.
(19) Schatzki, T. F. *J. Polym. Sci.* **1962**, *57*, 496.
(20) Schatzki, T. F. *Polym. Prepr. (Am. Chem. Soc., Div. Polym. Chem.)* **1965**, *6*, 646.
(21) Boyer, R. F. *Rubber Chem. Technol.* **1963**, *36*, 1303.
(22) Wunderlich, B. *J. Chem. Phys.* **1962** *37*, 2429.
(23) Tuijnman, C. A. F. *Polymer* **1963**, *4*, 259; **1963**, *4*, 315.
(24) Hoffman, J. D.; Williams, G.; Passaglia, E. *J. Polym. Sci., Part, C.* **1966**, *14*, 173.
(25) Mansfield, M. L.; Boyd, R. H. *J. Polym. Sci., Polym. Phys. Ed.* **1978**, *16*, 1227.
(26) Reneker, D. H. *J. Polym. Sci.* **1962**, *59*, S39.
(27) Reneker, D. H.; Fanconi, B. M.; Mazur, J. *J. Appl. Phys.* **1977**, *48*, 4032.
(28) Reneker, D. H.; Mazur, J. *Polymer* **1982**, *23*, 401.
(29) Reneker, D. H.; Mazur, J. *Polymer* **1983**, *24*, 1387.
(30) Reneker, D. H.; Mazur, J. *Polymer* **1988**, *29*, 3.
(31) Mansfield, M. L. *Chem. Phys. Lett.* **1980**, *69*, 383.
(32) Skinner, J. L.; Wolynes, P. G. *J. Chem. Phys.* **1980**, *73*, 4022.
(33) Skinner, J. L.; Park, Y. H. *Macromolecules* **1984**, *17*, 1735.
(34) Glasstone, S.; Laidler, K. J.; Eyring, H. *Theory of Rate Processes*; McGraw-Hill: New York, 1941.
(35) Sumpter, B. G.; Noid, D. W.; Wunderlich, B. *J. Chem. Phys.* **1990**, *93*, 6875.
(36) Sumpter, B. G.; Noid, D. W.; Wunderlich, B. *Macromolecules* **1992**, *25*, 7247.
(37) Sumpter, B. G.; Noid, D. W.; Liang, G. L. Wunderlich, B. *Adv. Polym. Sci.* **1994**, *116*, 27.
(38) Carbeck, J. D.; Rutledge, G. C. *Macromolecules* **1996**, *29*, 5190.
(39) Dodd, L. R.; Boone, T. D.; Theodorou, D. N. *Mol. Phys.* **1993**, *78*, 961.
(40) McMahon, P. E.; McCullough, R. L.; Schlegel, A. A. *J. Appl. Phys.* **1967**, *38*, 4123.
(41) Go, N.; Scheraga, H. A. *Macromolecules* **1970**, 3, 178.
(42) Pant, P. V. K.; Theodorou, D. N. *Macromolecules* **1995**, *28*, 7224.
(43) Mavrantas, V. G.; Boone, T. D.; Zervopoulou, E.; Theodorou, D. N. *Macromolecules* **1999**, *32*, 5072.
(44) Balijepalli, S.; Rutledge, G. C. *J. Chem. Phys.* **1998**, *109*, 6523.
(45) Balijepalli, S.; Rutledge, G. C. *Comput. Theor. Polym. Sci.* **2000**, *10*, 103.
(46) Gautam, S.; Balijepalli, S.; Rutledge, G. C. *Macromolecules* **2000**, *33*, 9136.
(47) Wu, M. G.; Deem, M. W. *J. Chem. Phys.* **1999**, *111*, 6625.
(48) Mowry, S. W.; Rutledge, G. C. Manuscript in preparation.
(49) Press, W. H.; Teukolsky, S. A.; Vetterling, W. T.; Flannery, B. P. *Numerical Recipes*; Cambridge University Press: Cambridge, U.K., 1992; Vol. 1.
(50) Sorensen, R. A.; Liau, W. B.; Kesner, L.; Boyd, R. H. *Macromolecules* **1988**, *21*, 200.
(51) Martonak, R.; Paul, W.; Binder, K. *J. Chem .Phys.* **1997**, *106*, 8918.
(52) Fischer, S. Karplus, M. *Chem. Phys. Lett.* **1992**, *194*, 252.
(53) Fukui, K. *Acc. Chem. Res.* **1981**, *14*, 363.
(54) Laidler, K. J. *Chemical Kinetics*, 3rd ed.; Harper Collins Publishers: New York, 1987.
(55) Murdoch, J. R. *J. Chem. Educ.* **1981**, *58*, 32.
(56) Parrinello, M.; Rahman, A. *J. Appl. Phys.* **1981**, *52*, 7182.
(57) Karasawa, N.; Goddard, W. A. *J. Phys. Chem.* **1989**, *93*, 7320.
(58) The asymmetry in the reaction pathway is the result of the finite length of the chain containing the defect in the calculation and the fact that local minima correspond to defect conformers located closer to one end or the other of the segment used in the CPR procedure.
(59) Schlegal, H. B. Optimization of Equilibrium Geometries and Transition Structures. In *Ab Initio Methods in Quantum Chemistry*; Lawley, K. P., Ed.; John Wiley and Sons: New York, 1987.

MA0118668